PCCP

Excited State Electronic Structure of Dimethyl Disulfide Involved in Photodissociation at ~200 nm

Journal:	*Physical Chemistry Chemical Physics*
Manuscript ID	CP-ART-06-2024-002505.R1
Article Type:	Paper
Date Submitted by the Author:	06-Aug-2024

Complete List of Authors:	Rishi, Varun; Sandia National Laboratories California, Combustion Research Facility Cole-Filipiak, Neil; Sandia National Laboratories California, Combustion Research Facility Ramasesha, Krupa; Sandia National Laboratories California, Gas Phase Chemical Physics McCaslin, Laura; Sandia National Laboratories California, Combustion Research Facility

Excited State Electronic Structure of Dimethyl Disulfide Involved in Photodissociation at ∼200 nm

Varun Rishi,[1] Neil C. Cole-Filipiak,[1] Krupa Ramasesha,[1, a)] and Laura M. McCaslin[1, b)]

Combustion Research Facility, Sandia National Laboratories, Livermore, California 94550, USA

(Dated: 27 August 2024)

Dimethyl disulfide (DMDS), one of the smallest organic molecules with an S-S bond, serves as a model system for understanding photofragmentation in polypeptides and proteins. Prior studies of DMDS photodissociation excited at ∼266 nm and ∼248 nm have elucidated the mechanisms of S-S and C-S bond cleavage, which involve the lowest excited electronic states S_1 and S_2. Far less is known about the dissociation mechanisms and electronic structure of relevant excited states of DMDS excited at ∼200 nm. Herein we present calculations of the electronic structure and properties of excited states S_1-S_6 accessed when DMDS is excited at ∼200 nm. Our analysis includes a comparison of theoretical and experimental UV spectra, as well as theoretically predicted one-dimensional cuts through the singlet and triplet potential energy surfaces along the S-S and C-S bond dissociation coordinates. Finally, we present calculations of spin-orbit coupling constants at the Franck-Condon geometry to assess the likelihood of ultrafast intersystem crossing. We show that choosing an accurate yet computationally efficient electronic structure method for calculating the S_0-S_6 potential energy surfaces along relevant dissociation coordinates is challenging due to excited states with doubly excited character and/or mixed Rydberg-valence character. Our findings demonstrate that the extended multi-state complete active space second-order perturbation theory (XMS-CASPT2) balances this computational efficiency and accuracy, as it captures both the Rydberg character of states in the Franck-Condon region and multiconfigurational character toward the bond-dissociation limits. We compare the performance of XMS-CASPT2 to a new variant of equation of motion coupled cluster theory with single, double, and perturbative triple corrections, EOM-CCSD(T)(a)*, finding that EOM-CCSD(T)(a)* significantly improves the treatment of doubly excited states compared to EOM-CCSD, but struggles to quantitatively capture asymptotic energies along bond dissociation coordinates for these states.

[a)]Electronic mail: kramase@sandia.gov

[b)]Electronic mail: lmmccas@sandia.gov

I. INTRODUCTION

Disulfide bonds play a necessary role in the conformational stability of proteins; the dynamics of their cleavage and formation can act as a switch for various protein functions.[1] Studying the gas phase photochemical dynamics of molecules with disulfide bonds after excitation in the ultraviolet (UV) range reveals the excited state dynamics underlying the competing photodissociation processes (S-S and C-S bond cleavage) in proteins and peptides.[2,3] Small organic compounds with S-S bonds are often used to model disulfide linkages between cysteine residues in proteins.[4–8]. One of the simplest organic molecules with a disulfide bond is dimethyl disulfide (DMDS).[9,10] In this work we focus on investigating the electronic structure of gas phase DMDS irradiated with ultraviolet (UV) light at $\sim$200 nm. To this aim, we benchmark electronic structure methods and subsequently characterize the nature of the states accessed in the excitation and photodissociation processes.

Previous studies of the gas phase photochemistry of DMDS indicate that UV irradiation of DMDS leads to the onset of dissociation through two major channels: one involving disulfide (S-S) bond cleavage leading to formation of thiomethoxy radicals (CH_3S) and another involving C-S bond dissociation, producing methyl perthiyl and methyl radicals (CH_3SS and CH_3, respectively):[10–19]

$$CH_3SSCH_3 \rightarrow CH_3S + CH_3S$$

$$CH_3SSCH_3 \rightarrow CH_3SS + CH_3$$

For excitation wavelengths of 248-266 nm (4.7-5.0 eV), formation of CH_3S radicals has long been thought to be the dominant photodissociation process.[11,14–17] This was confirmed in a recent study where DMDS was pumped at 267 nm and probed with time-resolved X-ray absorption spectroscopy; ultrafast S-S bond cleavage was observed, leading to formation of two thiomethoxy radicals (CH_3S) on a 120 $\pm$ 30 fs timescale.[10] The authors' supporting calculations employed complete active space second-order perturbation theory (CASPT2(10e,8o)) to identify that the lowest lying singlet excited state (S_1) are populated with 267 nm excitation through a transition from an S non-bonding orbital (n_S) to an anti-bonding σ^* orbital along the S-S bond, σ^*_{SS}. This study also provides evidence for asymmetric C-S dissociation ($\sim$30% yield), though the authors assign this pathway, at least in part, as resulting from multiphoton $\sim$266 nm absorption. In another study of $\sim$266 photodissociation of DMDS, Cao et al.[19] employed CASPT2(6e,4o) and a small basis set (6-31G* for S and 3-21G* for C and H) to compute the photodissociation dynamics

of DMDS using non-adiabatic mixed quantum-classical calculations. They found that most S-S bond cleavage occurs within 100 fs and also suggested that the system may undergo intersystem crossing (ISC) to the T_2 state along this dissociation pathway.

Compared to the breadth of work investigating the photophysical properties and dynamics of DMDS excited at ∼266 nm (∼4.7 eV), there have been far fewer studies of ∼200 nm (∼6.2 eV) excitation and photodissociation. To characterize the photodynamics after 193 nm (6.4 eV) excitation, three studies performed photofragment translational spectroscopy, finding both C-S and S-S bond dissociation channels.[14,20,21] CH_3S_2 fragments were found to undergo secondary dissociation to produce CH_3 and S_2.[14,21] Additionally, at this excitation energy, S-S dissociation was found to produce an valence excited CH_3S ($^2A_1$) radical.[14,21] While a few experimental studies on the excitation and photodissociation of DMDS at ∼200 nm have been performed, to the authors' knowledge, there are no corresponding theoretical studies characterizing the higher-lying electronic states along key dissociation coordinates.

Due to the few studies of DMDS at ∼200 nm excitation, there is incomplete analysis of Rydberg character in the S_1-S_6 electronic states. Tokue et al. reported absorption spectra of DMDS in the vacuum ultraviolet region, 100-220 nm (5.6-12.4 eV),[22] assigning numerous broad features to Rydberg states, including at 223 nm (5.6 eV). A theoretical study by Luo et al. assessed the Rydberg character of the excited states of DMDS by comparing their quadrupole moments to that of the ground state, finding that S_3-S_6 all exhibit significant Rydberg character.[18] However, visualization and analysis of these higher-lying states was outside the scope of their paper. We therefore aim to quantify the extent of Rydberg character and visualize the orbitals to assign key transitions relevant to the photodissociation at ∼200 nm.

Another key aim of this study is to evaluate electronic structure methods that can capture both the Rydberg character of states in the Franck-Condon region near 6 eV and the near degeneracies of states at the bond dissociation asymptotes. To assess the challenges associated with characterizing the bond breaking processes initiated when DMDS is excited at 200 nm, we present an analysis of the performance of excited state methods from the equation of motion coupled cluster (EOM-CC) and complete active space perturbation theory (CASPT2) families in predicting the excited state potential energy surfaces (PESs). To benchmark the methods' applicability in the Franck-Condon region, we compare calculated and experimental UV spectra, finding superior performance by equation of motion coupled cluster with single and double excitations (EOM-CCSD). To assess the methods' applicability at the bond dissociation asymptotes, we perform one

dimensional cuts through the PES along the two major dissociation coordinates: the C-S and S-S bonds. We highlight two particular challenges for electronic structure theory: (1) the presence of Rydberg character and (2) the presence of double excitation character in asymptotic regions of excited electronic states. We show how both of these challenges are somewhat mitigated by the EOM-CCSD(T)(a)* method which includes effects from triple excitations in addition to single and double excitations from EOM-CCSD. Though single-state CASPT2 based approaches are well suited for describing doubly excited states, they have been shown to struggle with the description of excited states of mixed Rydberg-valence character[23]. We demonstrate that the extended multi-state CASPT2 method (XMS-CASPT2) with an appropriate active space - 8 electrons in 8 orbitals (8e,8o) - balances the computational cost and accuracy needed to compute the excited states of DMDS in on-the-fly non-adiabatic dynamics calculations, which will be published in an upcoming study.

Based on the findings from our benchmarking, we present analysis and characterization of the electronic states involved in the photodissociation of DMDS at $\sim$200 nm. We quantify and characterize the role of Rydberg states in the Franck-Condon region. Furthermore, we present calculations of the spin-orbit coupling constants (SOCCs) of DMDS to assess the likelihood of ultrafast ISC. We also present cuts through the S_0-S_6 PESs and T_1-T_7 along the S-S and C-S bond dissociation coordinates to assess photofragmentation pathways, including those that may be accessible via ultrafast ISC. We find that both S-S and C-S bond dissociation may occur after $\sim$200 nm excitation.

II. METHODOLOGY

This section details the methodologies and software packages employed in the calculation and analysis of the electronic structure of DMDS. Primarily, we used the CFOUR[24], Q-Chem[25], and BAGEL[26] packages for their various specialized features. The ground state (S_0) geometry was optimized using coupled cluster theory with single, double and perturbative triple excitations (CCSD(T))[27] with the cc-pVDZ basis[28] in CFOUR. Excitation energies and oscillator strengths of the S_1-S_6 states at the equilibrium geometry were calculated with EOM-CCSD[29], and with triples correction, EOM-CCSD(T)(a)*[30], implemented in CFOUR. SOCCs were computed between singlet and triplet states employing EOM-CCSD/aug-cc-pVDZ. We also computed excitation energies using the multireference approach XMS-CASPT2[23,31–38] with active spaces 8 electrons in 8

orbitals (8e,8o) and 10 electrons in 10 orbitals (10e,10o) using the aug-cc-pVDZ basis and cc-pVQZ-jkfit basis for density fitting,[28,39,40] as implemented in BAGEL.[35] An imaginary shift of 0.2 atomic units was used for improved convergence of XMS-CASPT2 calculations.[41] The CASSCF orbitals used in the 8e,8o active space are selected as the 4 highest occupied and 4 lowest unoccupied orbitals and in the 10e,10o active space, the 5 highest occupied and 5 lowest unoccupied orbitals. While the character of the CASSCF orbitals necessarily change during bond dissociation, all of our calculations select the active space in this manner, which is a strategy amenable to computing molecular dynamics on-the-fly. We assess the quality of these active spaces by comparing the excitation energies along the S-S and C-S bond distances computed with each active space. Plots of the active orbitals of DMDS at its Franck-Condon geometry, as well as orbital characters can be found in SI, Figures S1 and S2.

Unrelaxed one-dimensional excited state PESs along the C-S and S-S bond stretches were computed using the EOM-CCSD and EOM-CCSD(T)(a)* levels of theory with the aug-cc-pVDZ basis. EOM-CCSD PES cuts are plotted alongside the S_0 state computed with coupled cluster theory with single and double excitations (CCSD).[42] EOM-CCSD(T)(a)* cuts are plotted alongside the S_0 state computed with a triples correction to CCSD, CCSD(T)(a).[30] XMS-CASPT2(8e,8o) and XMS-CASPT2(10e,10o) methods were also used to compute the one-dimensional PESs along these coordinates, employing the same basis as previously described for XMS-CASPT2. The T_1-T_7 one-dimensional PESs are also reported at the XMS-CASPT2(8e,8o) level of theory employing the same basis set and parameters as used for the singlet states. All XMS-CASPT2 calculations are based on state averaged CASSCF (SA-CASSCF) calculations for 7 singlet states or 7 triplet states. To characterize the nature of the S_1-S_6 states, natural transition orbitals (NTOs) were computed at the EOM-CCSD/aug-cc-pVDZ level of theory using Q-Chem version 5.4.2[25], and plotted using the Jmol software package.[43] The valence and Rydberg character of excited states were analyzed using their second moments[44] and expectation values of r^2. The $\langle r^2 \rangle$ values, which serve as a measure of diffuseness of the excited states compared to the ground state, were computed with EOM-CCSD/aug-cc-pVDZ in CFOUR.

III. RESULTS AND DISCUSSION

A. Benchmarking electronic structure methods in the Franck-Condon region

We present a benchmarking of theoretical methods employed; EOM-CCSD and XMS-CASPT2 are evaluated based on their performance computing vertical excitation energies and oscillator strengths for UV absorption spectra, which we compare to experiment. The experimental UV absorption spectra of DMDS, published by Hearn et al.[45] and Tokue et al.[22], exhibit a broad peak around 250 nm, a shoulder around 210 nm, and a more intense peak around 195 nm.[22,45,46] Thompson et al.[46] report that the broad peak at ∼250 nm is due to two close peaks arising from excitation into the S_1 and S_2 states. All methods studied find that both S_1 and S_2 are characterized by an $n_S \rightarrow \sigma^*_{SS}$ transition,[18] see Figure 6, Table II, and Section III.C.1 for more discussion. The identity of the first electronic state exhibiting Rydberg character has been a matter of debate. Tokue et al.[22] predict a Rydberg transition ($n_S \rightarrow 4s$) around 223 nm, though we do not identify such a feature here. Tokue et al. suggest that the peak at ∼195 nm corresponds to a non-Rydberg transition, though we find substantial Rydberg character in both S_5 and S_6 using all methods, as we show in Table II and discuss in more detail in Section III.C.1. All excited states S_1-S_6 have been previously assigned to the promotion of an n_S electron, aligning with our calculations.[10,18] We present excitation energies and oscillator strengths of transitions for the singlet states, $S_1 - S_6$, shown in Figure 1 and Table I. We note that the assignment of excited state character in XMS-CASPT2 is based on dominant CASSCF coefficient contributions, which are given in SI, Figures S1-S2 and Tables S1-S2. As we describe in Section III.C.1., quantification of the contributions of valence and Rydberg orbitals in XMS-CASPT2 calculations requires calculation of the expectation values $\langle r^2 \rangle$ between the XMS-CASPT2 wavefunctions, which is not currently implemented. We therefore assign these transitions qualitatively in the present work. All XMS-CASPT2 states S_3-S_6 computed with both active spaces exhibit mixtures of valence and Rydberg orbitals, though a quantitative assignment of these contributions is currently unavailable.

Figure 1 compares the theoretically predicted UV spectra with experiment. The spectrum computed with both EOM-CCSD and XMS-CASPT2(8e,8o) compare well with the experimental spectra based on our three-fold evaluation metric: the absolute energies of the most intense peaks as listed in Table I, the relative energies between the most intense peaks, and the agreement between theoretical oscillator strengths and their corresponding experimental peak intensity. In the EOM-

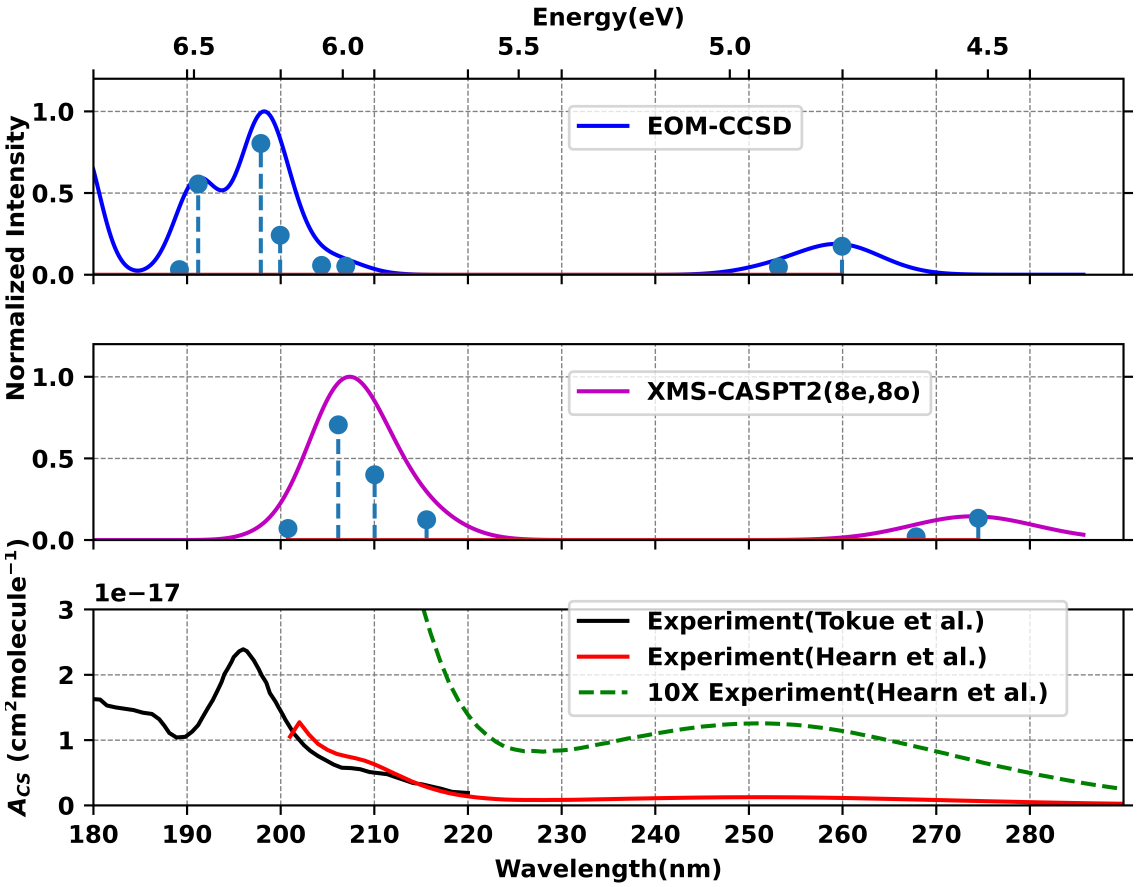

FIG. 1. A comparison of theoretical (EOM-CCSD, top, and XMS-CASPT2(8e,8o), middle) and experimental absorption spectra[22,45] (bottom). The dashed lines show the location of peaks in the theoretical spectra which have been uniformly broadened with peak full width at half maximum (FWHM) of 0.2 eV to resemble the experimental spectra. The highest intensity feature for the theoretical spectra are set to 1 and the absorption cross-section (A_{CS}) is in cm^{2}molecule^{-1} for the experimental spectra. A scaled version (10X magnified) of the experimental spectra by Hearn et al.[45] is included to enhance the broad peak in the 240-260 nm range.

CCSD spectrum, the most intense feature is the S_6 state at 197.9 nm, which is within 5 nm of the experimentally reported value. The XMS-CASPT2(8e,8o) calculation predicts that the transition with highest intensity is the S_5 state at 206 nm, while the S_6 state has an oscillator strength an order of magnitude smaller.

We compare the excitation energies and the oscillator strengths at the EOM-CCSD and XMS-CASPT2(8e,8o) levels of theory. We note that EOM-CCSD(T)(a)* is a method for triples-

TABLE I. The excitation energies (eV, nm) and the oscillator strengths (au) for the singlet excited states of DMDS at the EOM-CCSD and XMS-CASPT2(8e,8o) levels of theory. Excitation energies at the EOM-CCSD(T)(a)* level of theory are also reported.

State	Excitation Energy (eV)			Excitation Energy (nm)			Oscillator Strength (au)	
	EOM-CCSD	EOM-CCSD(T)(a)*	XMS-CASPT2(8e,8o)	EOM-CCSD	EOM-CCSD(T)(a)*	XMS-CASPT2(8e,8o)	EOM-CCSD	XMS-CASPT2(8e,8o)
S_1	4.77	4.69	4.52	259.9	264.4	274.3	0.009	0.008
S_2	4.90	4.81	4.63	253	257.8	267.8	0.003	0.001
S_3	6.00	5.92	5.75	206.6	209.4	215.6	0.004	0.007
S_4	6.07	6.00	5.90	204.3	206.6	210.1	0.003	0.022
S_5	6.20	6.14	6.01	200	201.9	206.3	0.013	0.040
S_6	6.27	6.20	6.17	197.7	200	200.9	0.042	0.004

TABLE II. The character of the excited states computed by EOM-CCSD, XMS-CASPT2(8e,8o), and XMS-CASPT2(10e,10o).

State	EOM-CCSD	XMS-CASPT2(8e,8o)	XMS-CASPT2(10e,10o)
S_1	$n_S \rightarrow \sigma^*_{SS}$	$n_S \rightarrow \sigma^*_{SS}$	$n_S \rightarrow \sigma^*_{SS}$
S_2	$n_S \rightarrow \sigma^*_{SS}$	$n_S \rightarrow \sigma^*_{SS}$	$n_S \rightarrow \sigma^*_{SS}$
S_3	$n_S \rightarrow$ Ryd.	$n_S \rightarrow$ Ryd. + σ^*_{CS}	$n_S \rightarrow$ Ryd. + σ^*_{CS}
S_4	$n_S \rightarrow$ Ryd.	$n_S \rightarrow$ Ryd. + σ^*_{CS}	$n_S \rightarrow$ Ryd. + σ^*_{CS}
S_5	$n_S \rightarrow$ Ryd. + σ^*_{CS}	$n_S \rightarrow$ Ryd. + σ^*_{CS}	$n_S \rightarrow$ Ryd. + σ^*_{CS}
S_6	$n_S \rightarrow$ Ryd. + σ^*_{CS}	$n_S \rightarrow$ Ryd. + σ^*_{CS}	$n_S \rightarrow$ Ryd. + σ^*_{CS}

correcting EOM-CCSD energies, which we report here; triples-corrected oscillator strengths cannot be computed with this method. EOM-CCSD predicts that both the S_5 and S_6 excited states are found to be most optically accessible at $\sim$200 nm, as evidenced by oscillator strengths larger than those of the optically accessible S_1 and S_2 states, see Table I and Figure 1. At the XMS-CASPT2(8e,8o) level of theory, the S_4 and S_5 states exhibit the largest oscillator strengths. In all cases, the EOM-CCSD and XMS-CASPT2(8e,8o) excitation energies are within 0.3 eV of one another. In Table I we also present a comparison of EOM-CCSD and EOM-CCSD(T)(a)* excitation energies, showing that at the Franck-Condon geometry, the triples correction of EOM-CCSD(T)(a)* only slightly improves the vertical excitation energies, with all triples corrected

values changing less than 0.1 eV. While XMS-CASPT2(8e,8o) is suitable for predicting the UV spectrum of DMDS, we find that EOM-CCSD achieves better performance in computing the absolute excitation energies. For this reason we choose EOM-CCSD for our analysis of the orbitals involved in electronic transitions in Section III.C.1.

B. Benchmarking electronic structure methods along dissociation pathways

In this subsection, we assess the performance of the electronic structure methods along the dissociation pathways by calculating ground and excited state PESs along the C-S and S-S bond coordinates. An adiabatic PES representation is used here, meaning that all intersections are represented as avoided crossings. Three methods, EOM-CCSD, EOM-CCSD(T)(a)* and XMS-CASPT2 using both (8e,8o) and (10e,10o) active spaces, are compared in order to establish a robust description of electron correlation at stretched geometries where the states exhibit multi-configurational character.[47–50]

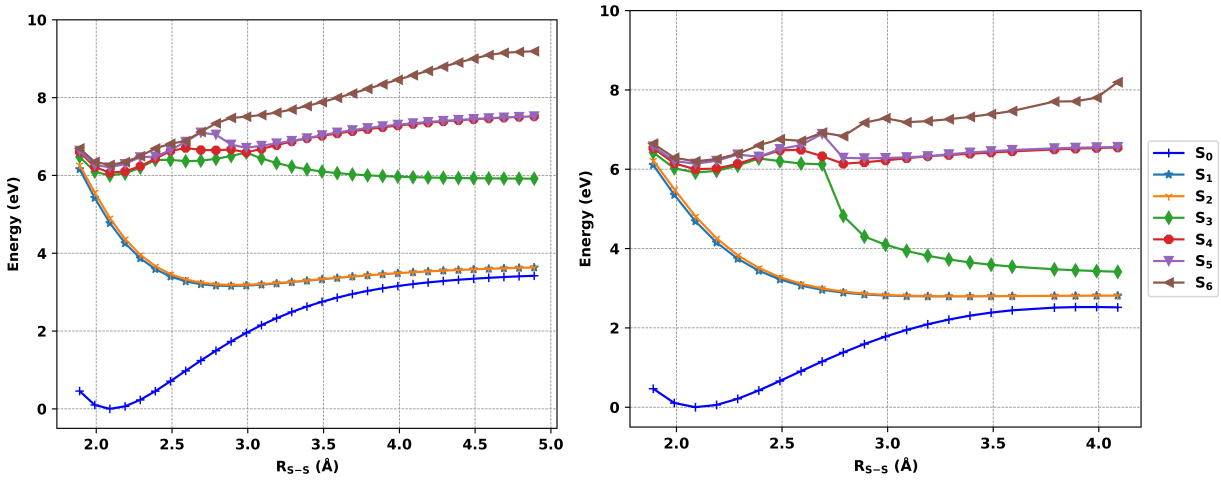

FIG. 2. The adiabatic PESs along the S-S bond coordinate using EOM-CCSD (left) and EOM-CCSD(T)(a)* (right) employing an aug-cc-pVDZ basis.

1. A comparison of excited state surfaces computed with EOM-CCSD, EOM-CCSD(T)(a) and XMS-CASPT2*

In the adiabatic PESs computed with EOM-CCSD/aug-cc-pVDZ, shown in Figure 2, states S_1 and S_2 are shown to be dissociative along the S-S coordinate for bond distances under 2.5Å. Along

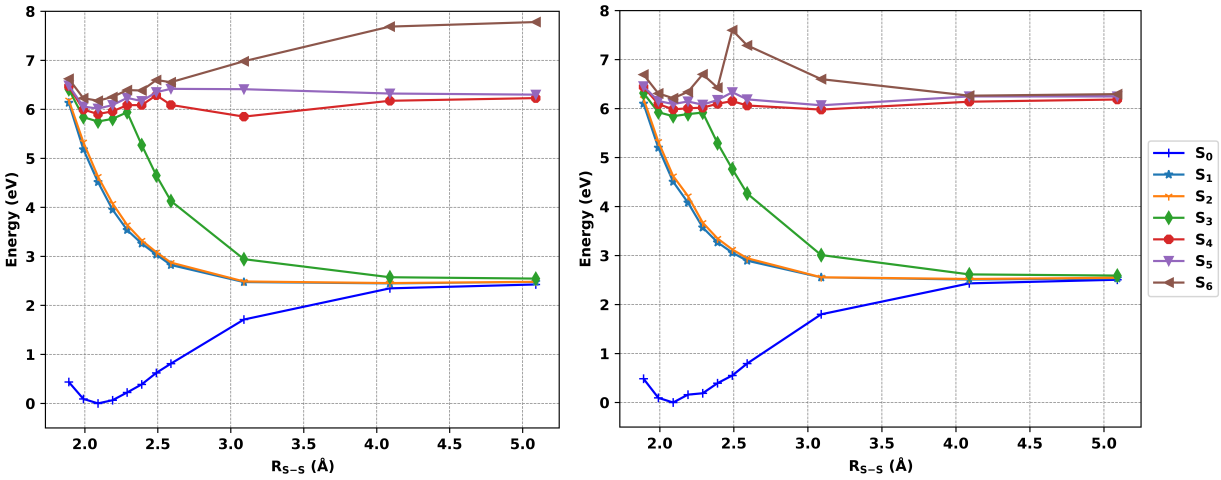

FIG. 3. The adiabatic PESs along the S-S bond dissociation coordinate using XMS-CASPT2(8e,8o) (left) and XMS-CASPT2(10e,10o) (right) employing an aug-cc-pVDZ basis.

this coordinate, both S_1 and S_2 exhibit a shallow well near 2.6Å. This is due to inadequate treatment of electron correlation in the EOM-CCSD method at stretched geometries, requiring inclusion of higher-order corrections. This is a well-studied problem in coupled cluster theory.[49,51–56] In contrast, the EOM-CCSD(T)(a)* method correctly predicts that states S_1 and S_2 are purely dissociative along the S-S stretch. This dissociative nature is due to the anti-bonding character of the lowest unoccupied MO (LUMO) of these states.[10,18] In Figure 3, we present the PESs along the S-S stretch computed with XMS-CASPT2(8e,8o) and XMS-CASPT2(10e,10o). These calculations also correctly show that S_1 and S_2 are purely dissociative along the S-S stretch.

Here we ascertain the suitability of our methods by comparing the asymptotic excited state energies with the corresponding experimental literature values. We note that these are cuts along the PESs are at fixed geometries and not relaxed on any state. Dissociation of DMDS along the S-S bond coordinate leads to two SCH_3S fragments. The S_0 state corresponds to dissociation of DMDS into two doublet ground state SCH_3 fragments, $^2E_{3/2}$. Martnez-Haya et al. measure this S_0 dissociation energy to be 2.8 eV.[21] CCSD overestimates this ground dissociation energy to be 3.2 eV. CCSD(T)(a) improves upon CCSD in calculation of the S_0 dissociation energy, yielding a value of 2.5 eV in slightly better agreement with the measured value. XMS-CASPT2(8e,8o) and XMS-CASPT2(10e,10o) both underestimate the S_0 dissociation energy, giving 2.3 and 2.4 eV, respectively.

The S_1-S_2 states correspond to dissociation into SCH_3 fragments where one fragment is in its

ground doublet state, $^2E_{3/2}$, and the other in its spin-orbit excited state, $^2E_{1/2}$. The spin-orbit splitting of these states is reported to be 0.032 eV.[57] The S_1 and S_2 S-S asymptotes are thus 0.03 eV above S_0. The S-S asymptote of the S_3 state corresponds to both SCH_3 fragments in $^2E_{1/2}$, 0.06 eV above S_0. Figure 2 shows that EOM-CCSD incorrectly predicts that the asymptotic limit of the S_3 state along the S-S coordinate is 2.7 eV higher than the S_0 asymptote. This issue is remedied somewhat by including triples corrections with EOM-CCSD(T)(a)*, as shown on the right panel of Figure 2. However, the asymptotic energy of the S_3 state computed with EOM-CCSD(T)(a)* is still 0.9 eV higher than that of the S_0 state, indicating that additional electron correlation is needed for proper treatment of this state exhibiting doubly excited character. In contrast to this, the cuts through the PES computed with XMS-CASPT2 with both the (8e,8o) and (10e,10o) active spaces exhibit approximately degenerate S_0-S_3 energies at the asymptotic limit, see Figure 3. We have performed an analysis of the S_3 XMS-CASPT2(8e,8o) wavefunction in terms of determinant coefficients (see Table **??** in supplementary info (SI)), which confirms the prominent double excitation character and necessitates methods with sufficient treatment of the states' multiconfigurational character.[38,56,58,59] If using an EOM-CC model, the inclusion of triples excitations is necessary, though we emphasize that further treatment of electron correlation is still needed to quantitatively treat the S_3 state of DMDS along the S-S dissociation coordinate.[30,60–62]

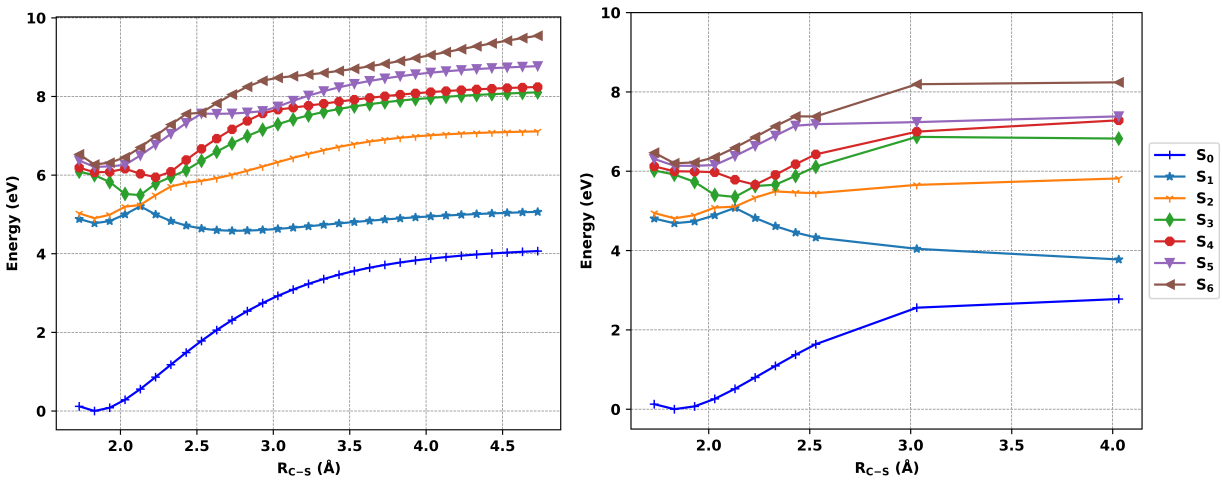

FIG. 4. The adiabatic PESs along the C-S bond coordinate using EOM-CCSD (left) and EOM-CCSD(T)(a)* (right) employing an aug-cc-pVDZ basis.

Figures 4 and 5 show the PESs along the C-S bond dissociation coordinate. For all levels of theory employed, the S_1 and S_2 states possess an energetic minimum along this coordinate close to

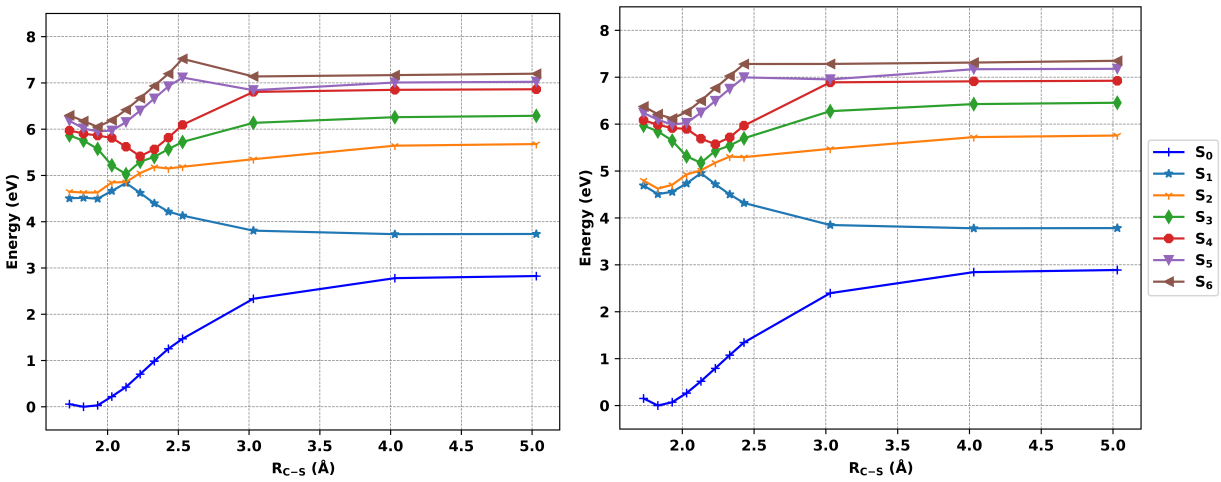

FIG. 5. The adiabatic PESs along the C-S bond dissociation coordinate using XMS-CASPT2(8e,8o) (left) and XMS-CASPT2(10e,10o) (right) employing an aug-cc-pVDZ basis.

the Franck-Condon geometry. The S_1 state exhibits a small barrier to dissociation, predicted to be 0.4 eV and 0.5 eV at the EOM-CCSD and XMS-CASPT2(10e,10o) levels of theory, respectively. Upon ~266 nm excitation to the S_1 state, the barrier along the C-S coordinate disfavors C-S dissociation relative to S-S dissociation (see Figure 2), contrasting with the conclusions of Ref.[17]. An important point of distinction between EOM-CCSD and the two other methods is the shape of the PES for the S_1 state at C-S bond distances of 2.5 Å< r < 3.5 Å. In this region, the S_1 state is predicted to be purely dissociative by EOM-CCSD(T)(a)* and XMS-CASPT2, while EOM-CCSD predicts a shallow well. This is similar to the issues found on the S_1 and S_2 states along the S-S dissociation coordinates, due to progressively increasing multi-reference character at the stretched limit and inadequate treatment of electron correlation with EOM-CCSD.

We now assess the performance of the different electronic structure methods by comparing C-S asymptotic energies with their experimental literature values. Martnez-Haya et al. report that the asymptote corresponding to DMDS dissociation into $SSCH_3$ and CH_3 is 2.4 eV.[21] CCSD significantly overestimates this bond dissociation energy to be 3.9 eV. CCSD(T)(a) calculates this energy to be 2.8 eV, which is a substantial improvement upon CCSD, indicating the need for higher-level treatment of electron correlation in the asymptotic region. XMS-CASPT2(8e,8o) and XMS-CASPT2(10e,10o) both give the same asymptotic energy as EOM-CCSD(T)(a)*, 2.8 eV.

Compared to the performance of EOM-CCSD at the S-S asymptotic limit, we find that EOM-CCSD and EOM-CCSD(T)(a)* are in better agreement with both XMS-CASPT2(8e,8o) and

XMS-CASPT2(10e,10o) at the C-S bond dissociation limit. In contrast to the S-S asymptotic energies, to our knowledge, there are no experimental measurements of excited state dissociation energies along the C-S bond. This is due to the instability of $SSCH_3$, which spontaneously decomposes into S_2 and CH_3 when produced with $\sim$2.1 eV of rovibrational energy.[21] We thus turn to EOM-CCSD/aug-cc-pVDZ calculations of the radical fragments to assess the performance of our methods at the asymptotes. We calculate the D_0-D_1 energy gap of $SSCH_3$ to be 0.9 eV and the D_0-D_1 energy gap of CH_3 to be 3.0 eV. Comparing the fragment energies with the asymptotic energies, we find that EOM-CCSD computes the S_0-S_1 and S_0-S_2 asymptotic energy gaps to be 1.1 and 3.1 eV, respectively, while EOM-CCSD(T)(a)* reports these values to be 1.0 and 3.0 eV. Because these curves are not relaxed along the C-S coordinates, we expect small differences in the asymptotic energies compared to the sums of the relaxed products. XMS-CASPT2(8e,8o) and XMS-CASPT2(10e,10o) both compute S_1 and S_2 asymptotic energies of 0.9 and 2.9 eV above S_0, respectively.

2. Discussion on challenges in computing the electronic structure in a computationally efficient manner for dynamics

One goal of this paper is to identify an excited state electronic structure method that balances accuracy and computational efficiency for non-adiabatic mixed quantum-classical dynamics. There are numerous challenges in finding such a method for computing electronic states S_0-S_6 in DMDS:

- **Doubly excited character of the S_3 excited state along the S-S stretch coordinate**: Along the S-S stretch coordinate, the S_3 state dissociates into two SCH_3 fragments, each in their spin-orbit excited states, $^2E_{1/2}$. This results in doubly excited character of the S_3 state along this coordinate. The single reference approach EOM-CCSD does not sufficiently treat electron correlation to account for this character, as evidenced by the significant difference between the stretched energies and sum of fragment energies in Table II. Addition of a triples correction using the framework of EOM-CCSD(T)(a)* helps in reducing the error in S_3 excitation energy but is not sufficient. This can be seen through the poor performance of EOM-CCSD(T)(a)* to describe the S_3 state's asymptotic energy along the S-S dissociation coordinate. Due to its multi-reference nature, XMS-CASPT2 correctly predicts the quasi-degeneracy of S_3 with the S_0-S_2 states at the S-S bond dissociation limit (see Figure 3). A discussion of the nature and weights of the Slater determinants in XMS-CASPT2 can be

found in the SI in Section S2.

- **Steep increase in computational expense with increase in active space**: The cost of multireference approaches such as XMS-CASPT2 depends on the the size of active space. Two major cost components in a XMS-CASPT2 calculation are the cost of CASSCF calculation and the second-order perturbative (PT2) correction. The cost of a CASSCF calculation scales exponentially with the size of the active space.[33,63] An on-the-fly excited state dynamics study of DMDS involves a large number of energy calculations as well as gradients. In this study we benchmark both (8e,8o) and (10e,10o) active spaces, finding that XMS-CASPT2 with an (8e,8o) active space sufficiently reproduces the electronic energies of the (10e,10o) active space along the two major bond-dissociation coordinates, as shown in Figures 4 and 6. Computational timings of single-point XMS-CASPT2 calculations employing both active spaces can be found in the SI, Table S3.

- **Describing mixed Rydberg-valence character of the S_5-S_6 excited states**: The XMS-CASPT2 approach with a diffuse basis set (aug-cc-pVDZ) is able to describe states with significant mixture of Rydberg and valence character as observed for S_5-S_6 of DMDS. State-specific (SS-CASPT2) approaches can struggle to treat states with Rydberg or mixed Rydberg-valence character.[23] We discuss this point in detail in the following section.

We find the challenges discussed above are satisfactorily dealt by a multi-reference multi-state approach such as XMS-CASPT2. Most importantly, the multi-configurational nature of this approach enables an accurate treatment of the doubly excited state (S_3 state along the S-S bond dissociation coordinate), where the EOM-CCSD method suffers from lack of static electron correlation.

C. Key insights on the electronic structure and photochemistry of DMDS

1. Characterizing the S_1-S_6 natural transition orbitals

We characterize the nature of the S_1-S_6 excited states by both qualitative and quantitative measures. We computed the highest occupied and lowest unoccupied NTOs (HONTOs and LUNTOs) using EOM-CCSD due to its superior performance in the Franck-Condon region. NTOs provide a single excitation picture for each excited state transition, often providing a single (or a small set

TABLE III. The expectation value, $\langle r^2 \rangle$ (in atomic units (au)), and $\Delta \langle r^2 \rangle$ (in au) for the ground and excited singlet states at EOM-CCSD/aug-cc-pVDZ level of theory.

State	$\langle r^2 \rangle$	$\Delta \langle r^2 \rangle$	Character
S_0	187.68		
S_1	189.02	1.34	Valence
S_2	188.96	1.28	Valence
S_3	200.24	12.56	Rydberg
S_4	198.33	10.65	Rydberg
S_5	193.72	6.04	Mixed Rydberg-valence
S_6	196.58	8.9	Mixed Rydberg-valence

of) dominant transitions from HONTO to LUNTO.[64] We note that an XMS-CASPT2 analogue of NTOs is not currently implemented in Bagel; we therefore assign the character of XMS-CASPT2 excited states qualitatively by identifying dominant CASSCF contributions, as described in Section III.A.In Figure 6 and 7, we plot the major NTOs for each excited state to characterize the dominant transitions. The LUNTOs for both S_1 and S_2 states are anti-bonding orbitals (σ^*_{SS}) with both HONTOs being characterized by n_S orbitals. For both S_1 and S_2, the HONTO $\rightarrow$ LUNTO transitions exhibit large single-excitation character of 95% and 96% respectively. S_3 exhibits Rydberg character, with the LUNTO characterized by a diffuse 4*s* Rydberg orbital. S_4 is a mixture of two transitions: HONTO $\rightarrow$ LUNTO (56%) and HONTO-1 $\rightarrow$ LUNTO+1 (39%). The LUNTO is a 4*s* Rydberg orbital and the LUNTO+1 is a 4*p* Rydberg orbital. Both S_4 HONTO and HONTO-1 are n_S orbitals. The LUNTOs for S_5 to S_6 have diffuse orbital character as well as valence character, leading us to characterize them as a mixture of valence and Rydberg character. S_5 is a mixture of two transitions: HONTO $\rightarrow$ LUNTO (87%) and HONTO-1 $\rightarrow$ LUNTO+1 (13%) where LUNTO and LUNTO+1 are 3*d* Rydberg orbital and σ^* C-S antibonding orbital, respectively. Similarly, the S_6 state is characterized by 76% HONTO $\rightarrow$ LUNTO and 24% HONTO-1 $\rightarrow$ LUNTO+1 transitions, where LUNTO and LUNTO+1 are characterized by a 3*d* Rydberg orbital and a σ^*_{CS} orbital, respectively. We thus find that the S_3-S_6 states all exhibit a degree of Rydberg character mixed with valence character from the σ^*_{CS} orbital, in agreement with conclusions from Luo et al.[18] and in contrast with Tokue.[22]

One way to quantify the Rydberg character of the excited states is by calculating the second

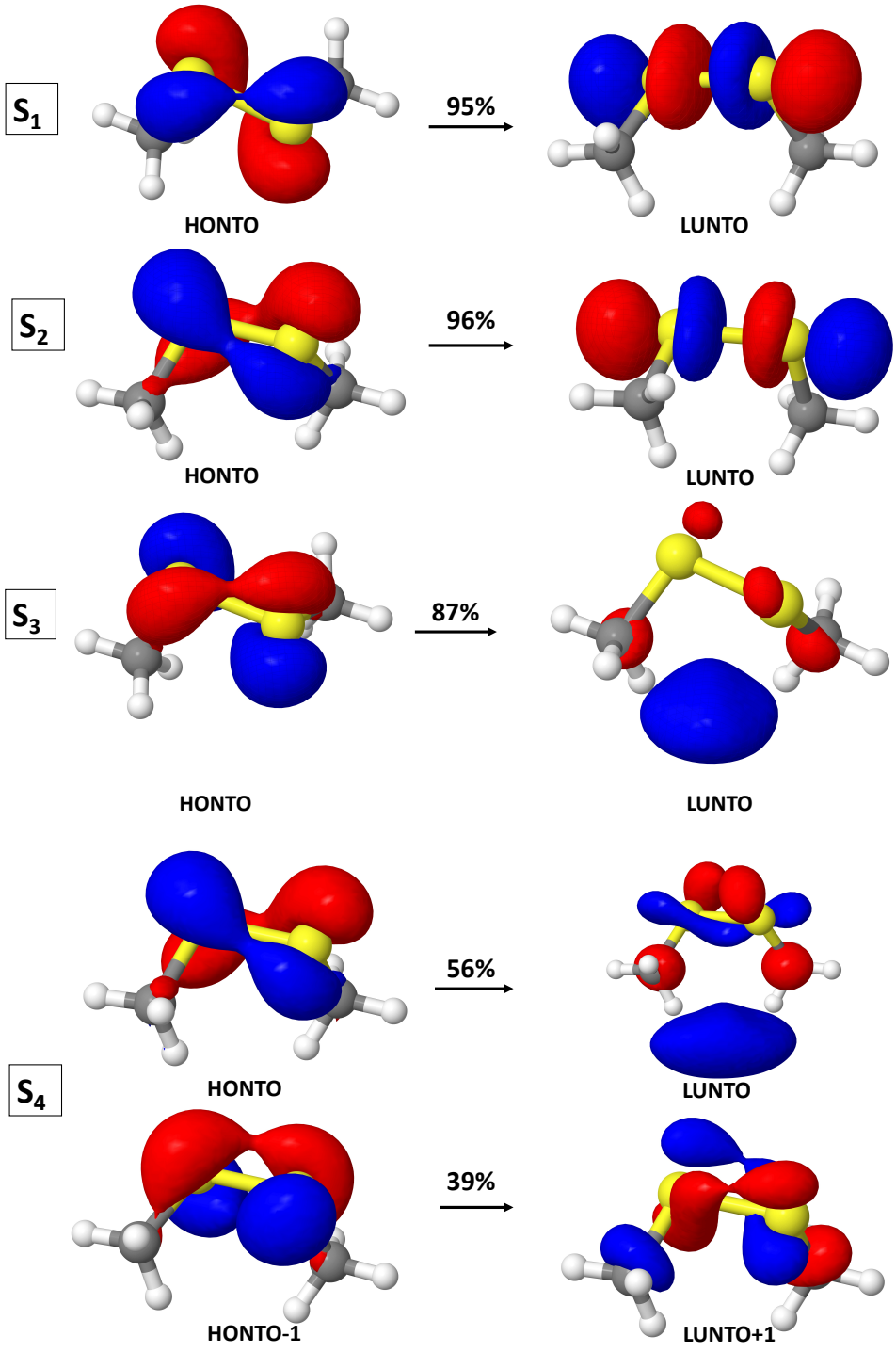

FIG. 6. NTOs for excited states $S_1 - S_4$ at the EOM-CCSD/aug-cc-pVDZ level of theory. An isodensity of 0.05 au was used for all plots except for those with diffuse Rydberg character, with isodensities in parentheses: LUNTO (0.035 au) of S_3, and LUNTO (0.03 au) of S_4, and LUNTO+1 (0.04 au) of S_4.

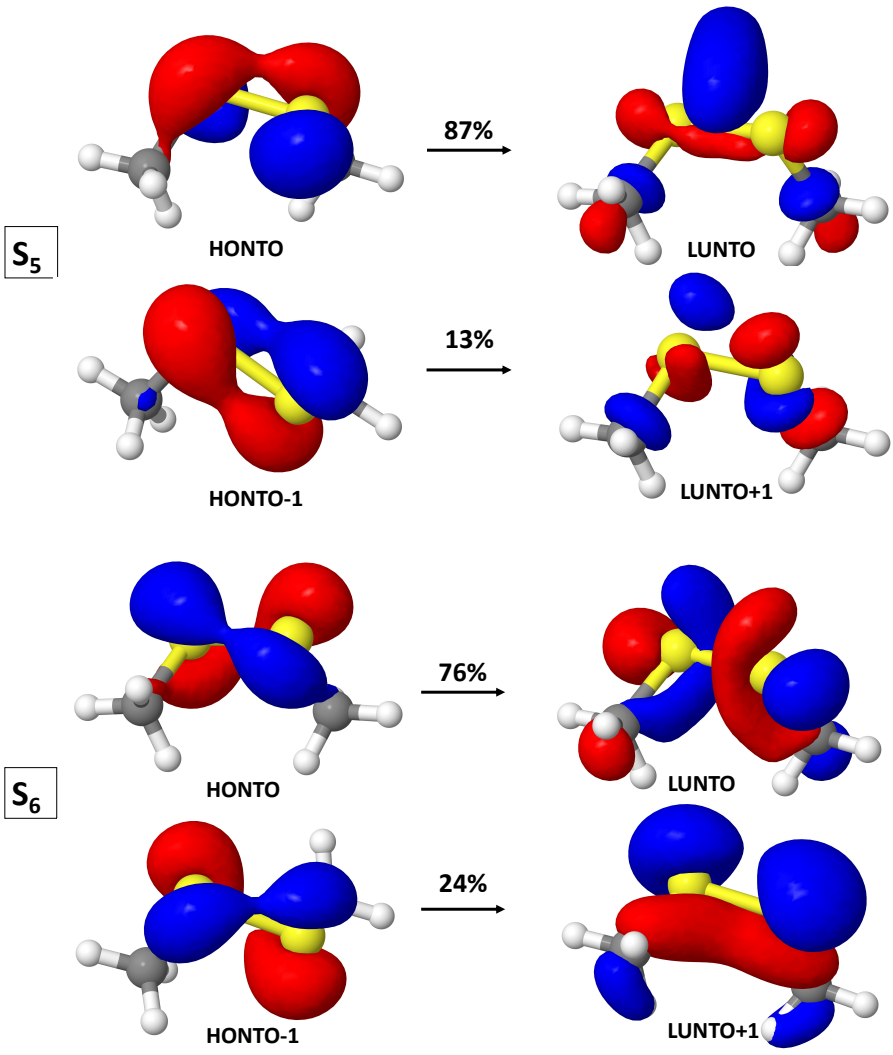

FIG. 7. NTOs for excited states S_5-S_6 at the EOM-CCSD/aug-cc-pVDZ level of theory. An isodensity of 0.05 au was used for all plots except for those with diffuse Rydberg character, with isodensities in parentheses: LUNTO (0.04 au) of S_5, LUNTO (0.035 au) of S_6, and LUNTO+1 (0.04 au) of S_6.

moments, $\langle r^2 \rangle$, of the excited state orbitals.[65] This quantity is used as a measure of the spatial extent of the electronic distribution.[44] The quantity $\Delta\langle r^2 \rangle$ is the difference in $\langle r^2 \rangle$ in the excited state electronic wavefunction compared to the ground state electronic wavefunction. This quantity helps us discriminate between Rydberg and valence excited states. Rydberg excited states are characterized by an excitation to a Rydberg orbital which is typically very diffuse with large spatial extent in contrast to orbitals of valence excited states.

$$\Delta\langle r^2\rangle = \langle r^2\rangle_{\text{excited state}} - \langle r^2\rangle_{\text{ground state}} \quad (1)$$

Table III reports the values of $\Delta\langle r^2\rangle$ for the excited states of DMDS studied using EOM-CCSD. We use $\Delta\langle r^2\rangle$ cutoffs of 0.0-1.9 for valence states, 2.0-10.0 for mixed valence-Rydberg states, and 10.0 for Rydberg states, in line with previous studies.[66] The valence excited states S_1 and S_2 show minimal change in $\langle r^2\rangle$ from the S_0 value. In S_3-S_6 we observe a significant change in the size of the excited state wavefunction compared to the ground state, as evidenced by the magnitude of $\Delta\langle r^2\rangle$. The S_3 state, due to a transition to a 4*s* Rydberg orbital, is the most diffuse of all states studied here, where $\langle r^2\rangle$ is $\sim$12 a_0^2 larger than its corresponding ground state value. S_4 is a mixture of two Rydberg transitions to 4*s* and 4*p* orbitals, and is also characterized by a large $\langle r^2\rangle$ of $\sim$11 a_0^2. States S_5 and S_6 have mixed Rydberg-valence character, evidenced by the NTO analysis discussed in the previous section and smaller $\Delta\langle r^2\rangle$. Each of these states is a mixture of at least two prominent excitations, a Rydberg transition to a 3*d* orbital and a valence transition to a σ^*_{CS} orbital.

2. Pathways to photodissociation through 1-dimensional PES cuts

We summarize here the important findings regarding the evolution of the molecular system out of the Franck-Condon region along two fragmentation pathways: the C-S and S-S bond dissociations, focusing on results from the XMS-CASPT2 calculations. Identifying mechanisms of dissociation at higher excitation energies is challenging due to the many electronic states involved, high dimensionality of the system, and numerous conical intersections. Upon excitation at $\sim$200 nm ($\sim$6.2 eV), states S_5 and S_6 can be accessed (see Figures 1 and Table I). From these states, both S-S and C-S bond cleavage are energetically accessible, as shown in Figures 3 and 5. One-dimensional cuts through the PESs along the C-S and S-S bond dissociation coordinates show pathways to the lowest of excited states, S_1 and S_2, via internal conversion (IC). Small stretches along the S-S and C-S coordinates show that IC is feasible in the vicinity of the Franck-Condon region due to numerous conical intersections, specifically at the contracted C-S bond length r < 1.8 Åand S-S bond length r < 2.0 Å, suggesting that IC will occur. We emphasize that these are proposed mechanisms based on 1D cuts through the PES. Full-dimensional non-adiabatic dynamics calculations are underway and will be presented in a follow-on study.

In the case of C-S bond breaking after excitation to S_5 or S_6, there is sufficient internal energy

undergo IC to the lowest excited state, S_1, whereby the molecule can dissociate, leading to the formation of CH_3SS and CH_3 fragments. While the production of electronically excited CH_3SS or CH_3 photoproducts has not been reported,[14,21] we note that the PESs in Figures 5 and 3 do not reflect the minimum energy pathway, as molecular geometries have not been relaxed along the reaction coordinate. Along the 1D C-S coordinate shown, dissociation in the S_2 state is energetically accessible upon 6.2 eV excitation, though the fraction of molecules that dissociate along this pathway is likely small.[21] Dissociation in the S_3-S_6 states is not energetically accessible; IC to S_1 and subsequent dissociation is the most likely pathway.

3. Assessment of ISC pathways

A previous theoretical study predicted that when DMDS is excited to its S_1 state, ISC is likely along the S-S dissociation coordinate.[19] However, as we have shown in section III.A, a highly correlated electronic structure method with sufficiently large active space is required for proper treatment of the potential energy surfaces along the dissociation coordinates, which was not employed in this previous study. Using our benchmarked electronic structure methods, we present high-level calculations of the SOCCs at the Franck-Condon geometry and one-dimensional cuts through the singlet and triplet PESs along the S-S and C-S bond coordinates to assess the likelihood of ultrafast ISC during photodissociation of DMDS. We note that intersystem crossing probabilities are dictated by both the SOCC and the singlet-triplet energy gap between the states. At present, our goal is to assess the likelihood of ISC through calculations of SOCCs at the Franck-Condon geometry and calculations of excited singlet and triplet state energies along the key dissociation coordinates. A thorough investigation of ISC timescales along these dissociation coordinates requires non-adiabatic dynamics calculations that include these singlet and triplet states and their SOCCs, which is outside the scope of this study.

Figure 8 presents the SOCCs between singlet and triplet states that may be accessed with $\sim$200 nm light. The magnitude of the SOCC is color-coded based on coupling strength, where dark green cells represent the mostly strongly spin-orbit coupled states and red represent the least coupled states. Pairs of states with SOCCs above 50 cm^{-1} are those that are strongly coupled enough that they may play a role in ultrafast ISC. The majority of these coupled singlet-triplet state pairs are lower-lying in energy, with S_0 strongly coupled to the three lowest triplet states. T_5 is also found to be strongly coupled to S_0-S_2. We again note that these values are computed the Franck-Condon

SOCC (cm^{-1})	S_0	S_1	S_2	S_3	S_4	S_5	S_6
T_1	103.8	18.1	76.1	15.1	12.0	15.3	7.3
T_2	124.1	63.8	4.5	6.2	22.6	13.1	7.5
T_3	145.0	21.7	21.1	7.7	2.3	10.2	7.4
T_4	16.7	26.0	20.0	8.6	19.1	1.5	28.1
T_5	105.0	118.3	127.4	34.5	13.7	39.8	1.0
T_6	33.2	6.5	5.1	7.0	30.6	4.6	63.3

FIG. 8. SOCCs of DMDS at the S_0 minimum, computed at the CCSD and EOM-CCSD/aug-cc-pVDZ levels of theory. Color codes range from green (large SOCC) to red (small SOCC).

geometry of DMDS. While ISC may occur in the Franck-Condon region, it may also occur during photodissociation along the fragmentation pathways. Future investigations of SOCCs and ISC rates along dissociation coordinates are certainly warranted given the significant number of large SOCCs in the Franck-Condon region, but these calculations are outside the scope of the present study.

Given the number of singlet-triplet state pairs with significant spin-orbit coupling in the Franck-Condon region, there is a possibility of ISC occurring during photodissociation of DMDS at $\sim$200 nm. To assess ISC mechanisms and pathways along the S-S and C-S dissociation coordinates, we report both singlet and triplet cuts along the PESs, shown in Figures 9 and 10. Along the S-S bond dissociation coordinate (see Figure 9), triplet states T_1-T_4 are all found to be quasi-degenerate with the S_0 asymptotic energy. In particular, T_4 is nearly degenerate with S_3 for S-S distances greater than $\sim$2.4 Å, which is a possible dissociation pathway for singlet dissociation. This quasi-degeneracy between S_3 and T_4 increases the likelihood of ISC along the S-S dissociation coordinate. Figure 10 presents the singlet and triplet state energies along the C-S bond dissociation coordinate. The T_2 state becomes nearly degenerate with S_1 at elongated C-S bond distances, which may serve as a pathway for ISC. The T_1 state becomes nearly degenerate with S_0 at elongated C-S bond distances. The T_1 state becomes nearly degenerate with T_2 and T_3 at $\sim$2.1 , connecting the excited state manifold to the ground singlet state. This near-degeneracy between T_1 and S_0 may also serve as a pathway for ISC, which is a possible explanation for the lack of previously reported excited state fragments in this channel. Based on the calculations presented here, there are numerous pathways where ISC is likely along both S-S and C-S dissociation coordinates.

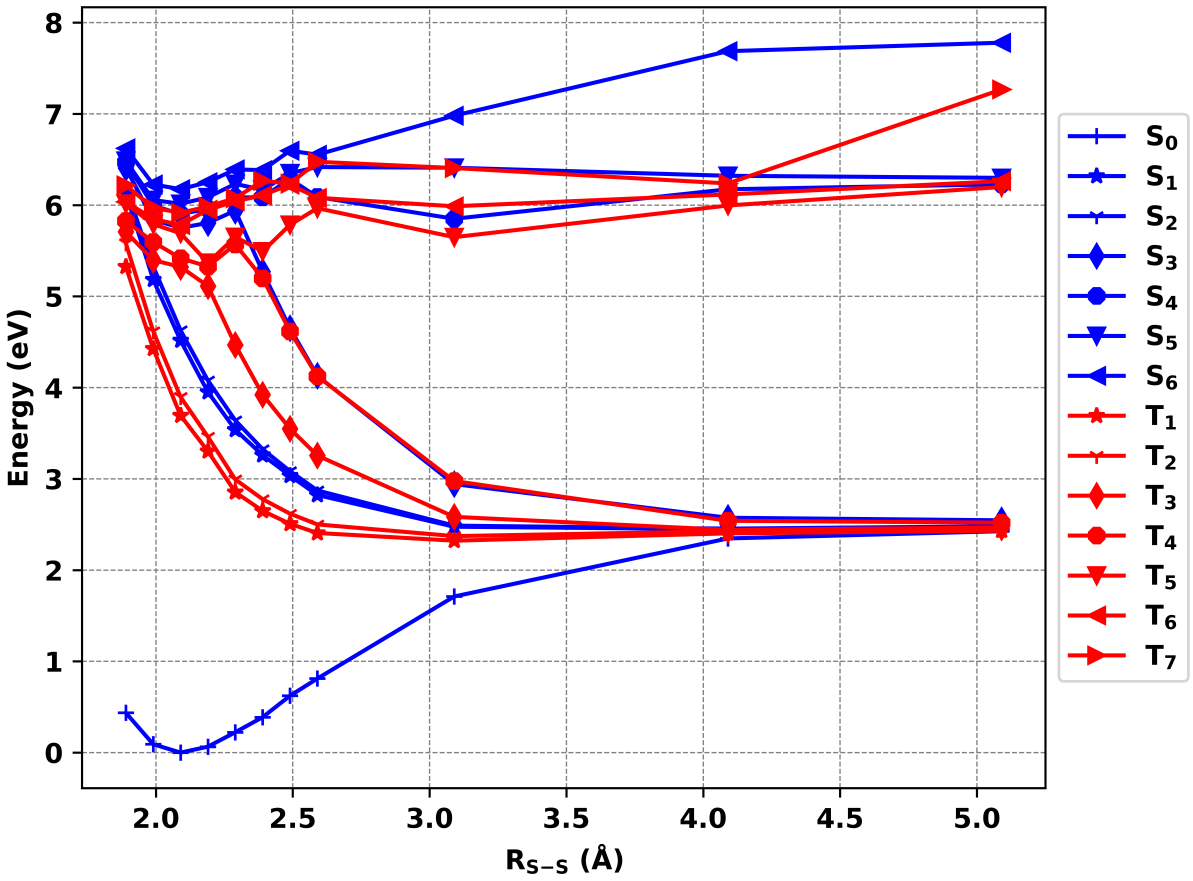

FIG. 9. The adiabatic PESs for singlet and triplet excited states along the S-S bond dissociation coordinate using XMS-CASPT2(8e,8o) employing an aug-cc-pVDZ basis.

IV. CONCLUSIONS

In this study, we computed the electronic structure of excited states involved in the photodissociation mechanisms of DMDS when excited at ∼200 nm. Our characterization of the excited states of DMDS employed EOM-CCSD, EOM-CCSD(T)(a)* and XMS-CASPT2 to assess the performance of two popular families of highly correlated methods for computing excited state energies and properties. We benchmarked computed UV spectra against experiment, finding that both EOM-CCSD and XMS-CASPT2 perform well and tackle the challenge of treating the Rydberg character of excited states in the Franck-Condon region, though EOM-CCSD achieves superior performance in computing absolute peak positions. We also benchmarked these methods by computing one-dimensional cuts through the PESs along the S-S and C-S bond dissociation coordinates. We find that along the S-S bond coordinate, EOM-CCSD fails in treating the double exci-

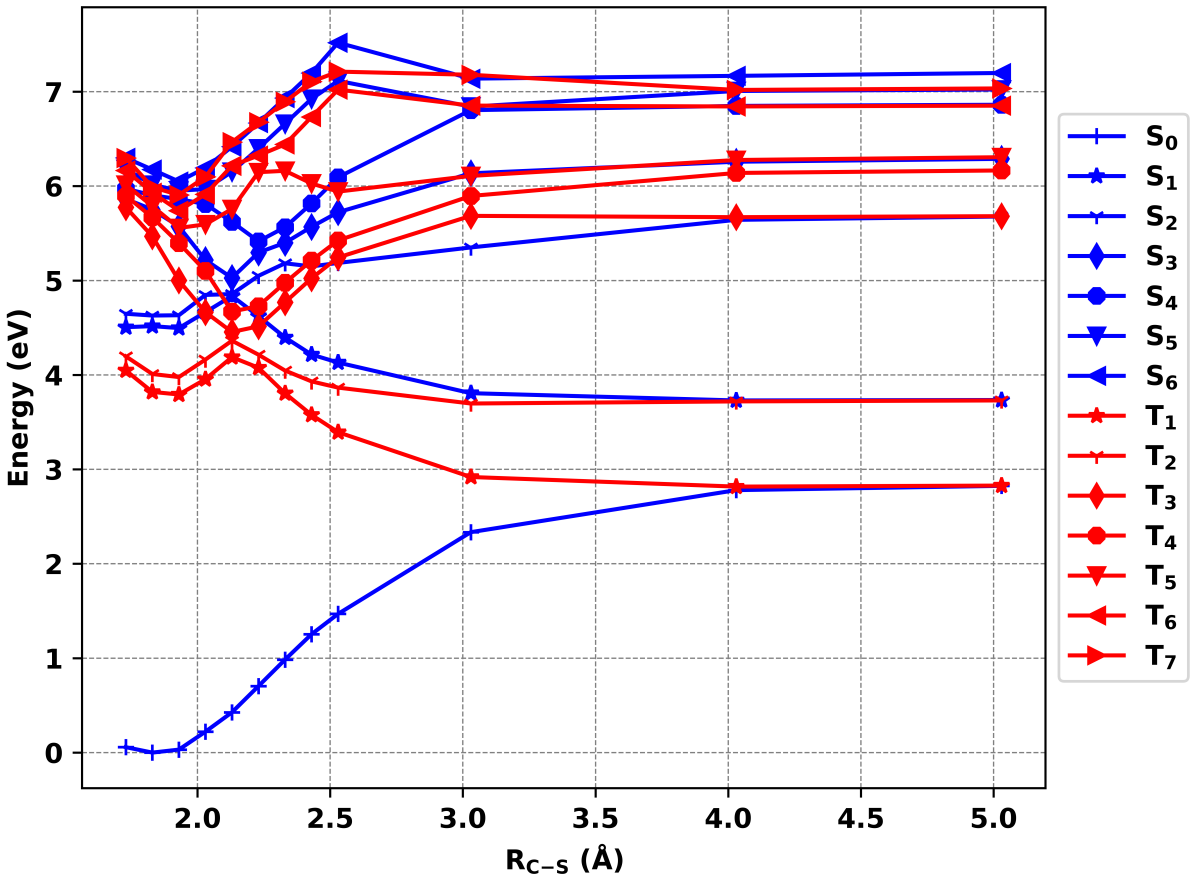

FIG. 10. The adiabatic PESs for singlet and triplet excited states along the C-S bond dissociation coordinate using XMS-CASPT2(8e,8o) employing an aug-cc-pVDZ basis.

tation character of the S_3 state; while this state should be quasi-degenerate with S_0, EOM-CCSD computes an S_0-S_3 asymptotic energy of 2.7 eV. The triples corrections of EOM-CCSD(T)(a)* reduces this error, computing an S_0-S_3 asymptotic energy of 0.9 eV. The multireference nature of XMS-CASPT2 enables great performance in the asymptotic region of S-S dissociation, as evidenced by its ability to predict quasi-degeneracy between states S_0-S_3. In assessing all three methods for computing energies in the Franck-Condon region, along the S-S dissociation pathway, and along the C-S dissociation pathway, we find that the XMS-CASPT2 performs the best overall. Furthermore, we find that an (8e,8o) active space for XMS-CASPT2 calculations balances accuracy and computational affordability for future non-adiabatic mixed quantum-classical dynamics calculations of these photodissociation pathways.

Using EOM-CCSD and XMS-CASPT2 in the Franck-Condon region and XMS-CASPT2 along

the dissociation coordinates, we propose viable pathways to S-S and C-S bond cleavages, as observed in experiments. We identify an accessible route from the ∼200 nm excited S_5-S_6 states to the S_3 state along the S-S bond coordinate. We propose that a series of IC events occur on an ultrafast timescale after initial excitation, and S-S dissociation on the dissociative S_3 state lead to the formation of SCH_3 radicals. Probing the C-S dissociation pathway by 1D PES calculations, we find that upon ∼200 nm excitation, there is sufficient internal energy to overcome small barriers, driving IC to the lowest excited state, S_1, upon which DMDS dissociates to CH_3SS and CH_3 fragments.

Finally, we present calculations of SOCCs at the Franck-Condon geometry to assess the likelihood of ultrafast ISC during photodissociation of DMDS. We find numerous SOCCs above 100 cm^{-1}, indicating that ultrafast ISC may occur. We therefore computed singlet and triplet PESs along the S-S and C-S bond dissociation coordinates. Along the S-S dissociation coordinate, T_1-T_4 become quasi-degenerate with the S_0 state. Along the C-S dissociation coordinate, we find that the T_1 state becomes quasi-degenerate with the S_0 state, unlike the excited singlet states, which may act as a connection between the excited states and ground state via ISC.

V. ACKNOWLEDGEMENTS

The Gas Phase Chemical Physics Program in the The Division of Chemical Sciences, Geosciences and Biosciences, Office of Basic Energy Sciences (BES), U.S. Department of Energy (USDOE) supported V.R., N.C.C.-F., K.R., and L.M.M. This research used resources of the National Energy Research Scientific Computing Center, a DOE Office of Science User Facility supported by the Office of Science of the U.S. Department of Energy under Contract No. DE-AC02-05CH11231 using NERSC award BES-ERCAP0029923. Sandia National Laboratories is a multimission laboratory managed and operated by National Technology and Engineering Solutions of Sandia, LLC (NTESS), a wholly owned subsidiary of Honeywell International Inc., for the U.S. Department of Energy's National Nuclear Security Administration (DOE/NNSA) under contract DE-NA0003525. This written work is authored by an employee of NTESS. The employee, not NTESS, owns the right, title and interest in and to the written work and is responsible for its contents. Any subjective views or opinions that might be expressed in the written work do not necessarily represent the views of the U.S. Government. The publisher acknowledges that the U.S. Government retains a non-exclusive, paid-up, irrevocable, world-wide license to publish or reproduce the

REFERENCES

[1]P. J. Hogg, *Trends in Biochemical Sciences*, 2003, **28**, 210–214.

[2]D. Creed, *Photochemistry and Photobiology*, 1984, **39**, 577–583.

[3]Y. M. E. Fung, F. Kjeldsen, O. A. Silivra, T. W. D. Chan and R. A. Zubarev, *Angewandte Chemie International Edition*, 2005, **44**, 6399–6403.

[4]T. E. Creighton, *BioEssays*, 1988, **8**, 57–63.

[5]W. J. Wedemeyer, E. Welker, M. Narayan and H. A. Scheraga, *Biochemistry*, 2000, **39**, 4207–4216.

[6]T. J. Bechtel and E. Weerapana, *PROTEOMICS*, 2017, **17**, 1600391.

[7]A. B. Stephansen, M. A. Larsen, L. B. Klein and T. I. Sølling, *Chem. Phys.*, 2014, **442**, 77–80.

[8]M. A. B. Larsen, A. B. Skov, C. M. Clausen, J. Ruddock, B. Stankus, P. M. Weber and T. I. Sølling, *ChemPhysChem*, 2018, **19**, 2829–2834.

[9]V. Renugopalakrishnan and R. Walter, *Zeitschrift für Naturforschung A*, 1984, **39**, 495–498.

[10]K. Schnorr, A. Bhattacherjee, K. J. Oosterbaan, M. G. Delcey, Z. Yang, T. Xue, A. R. Attar, A. S. Chatterley, M. Head-Gordon, S. R. Leone and O. Gessner, *J. Phys. Chem. Lett.*, 2019, **10**, 1382–1387.

[11]P. M. Rao, J. A. Copeck and A. R. Knight, *Can. J. Chem.*, 1967, **45**, 1369–1374.

[12]A. B. Callear and D. R. Dickson, *Trans. Faraday Soc.*, 1970, **66**, 1987–1995.

[13]A. Kumar, P. K. Chowdhury, K. V. S. Rama Rao and J. P. Mittal, *Chem. Phys. Lett.*, 1992, **198**, 406–412.

[14]Y. R. Lee, C. L. Chiu and S. M. Lin, *J. Chem. Phys.*, 1994, **100**, 7376–7384.

[15]C. Hsu and C. Y. Ng, *J. Chem. Phys.*, 1994, **101**, 5596–5603.

[16]C. W. Bookwalter, D. L. Zoller, P. L. Ross and M. V. Johnston, *Journal of the American Society for Mass Spectrometry*, 1995, **6**, 872–876.

[17]A. Rinker, C. D. Halleman and M. R. Wedlock, *Chem. Phys. Lett.*, 2005, **414**, 505–508.

[18]C. Luo, W.-N. Du, X.-M. Duan, J.-Y. Liu and Z.-S. Li, *Chem. Phys. Lett.*, 2009, **469**, 242–246.

[19]J. Cao and D.-C. Chen, *Phys. Chem. Chem. Phys.*, 2019, **21**, 4176–4183.

[20]S. Nourbakhsh, C. Liao and C. Y. Ng, *J. Chem. Phys.*, 1990, **92**, 6587–6593.

[21]B. Martińez-Haya, M. J. Bass, M. Brouard, C. Vallance, I. Torres and J. Barr, *J. Chem. Phys.*, 2004, **120**, 11042–11052.

[22]I. Tokue, A. Hiraya and K. Shobatake, *Chem. Phys.*, 1989, **130**, 401–408.

[23]J. Finley, P.- Malmqvist, B. O. Roos and L. Serrano-Andrés, *Chem. Phys. Lett.*, **288**, 299–306.

[24]D. A. Matthews, L. Cheng, M. E. Harding, F. Lipparini, S. Stopkowicz, T.-C. Jagau, P. G. Szalay, J. Gauss and J. F. Stanton, *J. Chem. Phys.*, 2020, **152**, 214108.

[25]E. Epifanovsky, A. T. B. Gilbert, X. Feng, J. Lee, Y. Mao, N. Mardirossian, P. Pokhilko, A. F. White, M. P. Coons, A. L. Dempwolff, Z. Gan, D. Hait, P. R. Horn, L. D. Jacobson, I. Kaliman, J. Kussmann, A. W. Lange, K. U. Lao, D. S. Levine, J. Liu, S. C. McKenzie, A. F. Morrison, K. D. Nanda, F. Plasser, D. R. Rehn, M. L. Vidal, Z.-Q. You, Y. Zhu, B. Alam, B. J. Albrecht, A. Aldossary, E. Alguire, J. H. Andersen, V. Athavale, D. Barton, K. Begam, A. Behn, N. Bellonzi, Y. A. Bernard, E. J. Berquist, H. G. A. Burton, A. Carreras, K. Carter-Fenk, R. Chakraborty, A. D. Chien, K. D. Closser, V. Cofer-Shabica, S. Dasgupta, M. de Wergifosse, J. Deng, M. Diedenhofen, H. Do, S. Ehlert, P.-T. Fang, S. Fatehi, Q. Feng, T. Friedhoff, J. Gayvert, Q. Ge, G. Gidofalvi, M. Goldey, J. Gomes, C. E. González-Espinoza, S. Gulania, A. O. Gunina, M. W. D. Hanson-Heine, P. H. P. Harbach, A. Hauser, M. F. Herbst, M. Hernández Vera, M. Hodecker, Z. C. Holden, S. Houck, X. Huang, K. Hui, B. C. Huynh, M. Ivanov, Jász, H. Ji, H. Jiang, B. Kaduk, S. Kähler, K. Khistyaev, J. Kim, G. Kis, P. Klunzinger, Z. Koczor-Benda, J. H. Koh, D. Kosenkov, L. Koulias, T. Kowalczyk, C. M. Krauter, K. Kue, A. Kunitsa, T. Kus, I. Ladjánszki, A. Landau, K. V. Lawler, D. Lefrancois, S. Lehtola, R. R. Li, Y.-P. Li, J. Liang, M. Liebenthal, H.-H. Lin, Y.-S. Lin, F. Liu, K.-Y. Liu, M. Loipersberger, A. Luenser, A. Manjanath, P. Manohar, E. Mansoor, S. F. Manzer, S.-P. Mao, A. V. Marenich, T. Markovich, S. Mason, S. A. Maurer, P. F. McLaughlin, M. F. S. J. Menger, J.-M. Mewes, S. A. Mewes, P. Morgante, J. W. Mullinax, K. J. Oosterbaan, G. Paran, A. C. Paul, S. K. Paul, F. Pavošević, Z. Pei, S. Prager, E. I. Proynov, Rák, E. Ramos-Cordoba, B. Rana, A. E. Rask, A. Rettig, R. M. Richard, F. Rob, E. Rossomme, T. Scheele, M. Scheurer, M. Schneider, N. Sergueev, S. M. Sharada, W. Skomorowski, D. W. Small, C. J. Stein, Y.-C. Su, E. J. Sundstrom, Z. Tao, J. Thirman, G. J. Tornai, T. Tsuchimochi, N. M. Tubman, S. P. Veccham, O. Vydrov, J. Wenzel, J. Witte, A. Yamada, K. Yao, S. Yeganeh, S. R. Yost, A. Zech, I. Y. Zhang, X. Zhang, Y. Zhang, D. Zuev, A. Aspuru-Guzik, A. T. Bell, N. A. Besley, K. B. Bravaya, B. R. Brooks, D. Casanova, J.-D. Chai, S. Coriani, C. J. Cramer, G. Cserey, A. E. DePrince, R. A. DiStasio, A. Dreuw, B. D.

Dunietz, T. R. Furlani, W. A. Goddard, S. Hammes-Schiffer, T. Head-Gordon, W. J. Hehre, C.-P. Hsu, T.-C. Jagau, Y. Jung, A. Klamt, J. Kong, D. S. Lambrecht, W. Liang, N. J. Mayhall, C. W. McCurdy, J. B. Neaton, C. Ochsenfeld, J. A. Parkhill, R. Peverati, V. A. Rassolov, Y. Shao, L. V. Slipchenko, T. Stauch, R. P. Steele, J. E. Subotnik, A. J. W. Thom, A. Tkatchenko, D. G. Truhlar, T. Van Voorhis, T. A. Wesolowski, K. B. Whaley, H. L. Woodcock, P. M. Zimmerman, S. Faraji, P. M. W. Gill, M. Head-Gordon, J. M. Herbert and A. I. Krylov, *J. Chem. Phys.*, 2021, **155**, 084801.

[26]T. Shiozaki, *WIREs Comput Mol Sci.*, 2018, **8**, e1331.

[27]K. Raghavachari, G. W. Trucks, J. A. Pople and M. Head-Gordon, *Chem. Phys. Lett.*, 1989, **157**, 479.

[28]T. H. Dunning, *J. Chem. Phys.*, 1989, **90**, 1007–1023.

[29]J. F. Stanton and R. J. Bartlett, *J. Chem. Phys.*, 1993, **98**, 7029.

[30]D. A. Matthews and J. F. Stanton, *J. Chem. Phys.*, 2016, **145**, 124102.

[31]B. O. Roos, P. R. Taylor and P. E. Sigbahn, *Chem. Phys.*, 1980, **48**, 157–173.

[32]K. Andersson, P. A. Malmqvist, B. O. Roos, A. J. Sadlej and K. Wolinski, *J. Phys. Chem.*, 1990, **94**, 5483–5488.

[33]S. Battaglia, I. Fdez. Galván and R. Lindh, *Theoretical and Computational Photochemistry*, Elsevier, 2023, pp. 135–162.

[34]A. A. Granovsky, *J. Chem. Phys.*, 2011, **134**, 214113.

[35]T. Shiozaki, W. Győrffy, P. Celani and H.-J. Werner, *J. Chem. Phys.*, 2011, **135**, 081106.

[36]B. Vlaisavljevich and T. Shiozaki, *J. Chem. Theory Comput.*, 2016, **12**, 3781–3787.

[37]J. W. Park and T. Shiozaki, *J. Chem. Theory Comput.*, 2017, **13**, 2561–2570.

[38]J. W. Park, R. Al-Saadon, M. K. MacLeod, T. Shiozaki and B. Vlaisavljevich, *Chem. Rev.*, 2020, **120**, 5878–5909.

[39]R. A. Kendall, T. H. Dunning and R. J. Harrison, *J. Chem. Phys.*, 1992, **96**, 6796–6806.

[40]D. E. Woon and T. H. Dunning, *J. Chem. Phys.*, 1993, **98**, 1358–1371.

[41]N. Forsberg and P. Åke Malmqvist, *Chemical Physics Letters*, 1997, **274**, 196–204.

[42]I. Purvis, George D. and R. J. Bartlett, *J. Chem. Phys.*, 1982, **76**, 1910–1918.

[43]*Jmol: an open-source Java viewer for chemical structures in 3D. http://www.jmol.org/*, `http://jmol.sourceforge.net/`.

[44]J. B. Foresman, M. Head-Gordon, J. A. Pople and M. J. Frisch, *J. Phys. Chem.*, 1992, **96**, 135–149.

[45]C. H. Hearn, E. Turcu and J. A. Joens, *Atmospheric Environment. Part A. General Topics*, 1990, **24**, 1939–1944.

[46]S. D. Thompson, D. G. Carroll, F. Watson, M. O'Donnell and S. P. McGlynn, *J. Chem. Phys.*, 1966, **45**, 1367–1379.

[47]D. Robinson, *J. Comp. Chem.*, 2013, **34**, 2625–2634.

[48]C. J. Stein, V. von Burg and M. Reiher, *J. Chem. Theory Comput.*, 2016, **12**, 3764–3773.

[49]V. Rishi, A. Perera and R. J. Bartlett, *J. Chem. Phys.*, 2016, **144**, 124117.

[50]R. J. Bartlett, *Int. J. Mol. Sc.*, 2002, **3**, 579–603.

[51]W. D. Laidig, P. Saxe and R. J. Bartlett, *J. Chem. Phys.*, 1987, **86**, 887–907.

[52]X. Li and J. Paldus, *J. Chem. Phys.*, 1998, **108**, 637–648.

[53]K. R. Yang, A. Jalan, W. H. Green and D. G. Truhlar, *Journal of Chemical Theory and Computation*, 2013, **9**, 418–431.

[54]I. W. Bulik, T. M. Henderson and G. E. Scuseria, *J. Chem. Theor. Comput.*, 2015, **11**, 3171.

[55]F. A. Evangelista, *J. Chem. Phys.*, 2011, **134**, 224102.

[56]A. Tajti, J. F. Stanton, D. A. Matthews and P. G. Szalay, *J. Chem. Theory Comput.*, 2018, **14**, 5859–5869.

[57]S. Chiang and Y. Lee, *J. Chem. Phys.*, 1991, **95**, 66–72.

[58]H. Lischka, D. Nachtigallová, A. J. A. Aquino, P. G. Szalay, F. Plasser, F. B. C. Machado and M. Barbatti, *Chemical Reviews*, 2018, **118**, 7293–7361.

[59]S. Gozem, F. Melaccio, A. Valentini, M. Filatov, M. Huix-Rotllant, N. Ferré, L. M. Frutos, C. Angeli, A. I. Krylov, A. A. Granovsky, R. Lindh and M. Olivucci, *Journal of Chemical Theory and Computation*, 2014, **10**, 3074–3084.

[60]P.-F. Loos, F. Lipparini, M. Boggio-Pasqua, A. Scemama and D. Jacquemin, *J. Chem. Theory Comput.*, 2020, **16**, 1711–1741.

[61]K. Boguslawski, *J. Chem. Theory Comput.*, 2019, **15**, 18–24.

[62]V. Rishi, M. Ravi, A. Perera and R. J. Bartlett, *J. Phys. Chem. A*, 2023, **127**, 828–834.

[63]J. Olsen, *International Journal of Quantum Chemistry*, 2011, **111**, 3267–3272.

[64]R. L. Martin, *J. Chem. Phys.*, 2003, **118**, 4775–4777.

[65]M. Nooijen and R. J. Bartlett, *J. Chem. Phys.*, 1997, **106**, 6441–6448.

[66]H. Reisler and A. I. Krylov, *Int. Rev. Phys. Chem.*, 2009, **28**, 267–308.

Data Availability

The authors will provide all data used to support the study in the form of output files from electronic structure codes in a public and free-of-cost online database upon acceptance of the paper.